TRENDS IN SCIENCES 2025; 22(10): 10418
https://doi.org/10.48048/tis.2025.10418 RESEARCH ARTICLE

Antibacterial Hydrogel Films Embedded with Cu–Ag Oxide Nanoparticles Based on Basil Seed Mucilage for Advanced Wound Dressing Applications

Jiyapa Sripirom[1], Rungrudee Srisomang[1], Sakuntala Siri-Udom[2], Cybelle Morales Futalan[3], Khongvit Prasitnok[4], Orrasa Prasitnok[4], Sirilak Kamonwannasit[5], Agarat Kamcharoen[5], Pongtanawat Khemthong[6] and Piaw Phatai[1,*]

[1]Department of Chemistry, Faculty of Science, Udon Thani Rajabhat University, Udon Thani 41000, Thailand
[2]Department of Biology, Faculty of Science, Udon Thani Rajabhat University, Udon Thani 41000, Thailand
[3]Institute of Civil Engineering, University of the Philippines Diliman, Quezon City 1101, Philippines
[4]Department of Chemistry, Faculty of Science, Mahasarakham University, Maha Sarakham 44150, Thailand
[5]Department of Agro-Industrial Product Development, Faculty of Agricultural Technology, Burapha University, Sakaeo 27160, Thailand
[6]National Nanotechnology Center (NANOTEC), National Science and Technology Development Agency (NSTDA), Pathum Thani 12120, Thailand

([*]Corresponding author's e-mail: piaw.ph@udru.ac.th)

Received: 21 April 2025, Revised: 26 May 2025, Accepted: 5 June 2025, Published: 15 July 2025

Abstract

Hydrogel films with antibacterial properties, swelling capability, and mechanical strength show promise as wound dressings. This study investigates the fabrication of $Cu_{1.0-x}Ag_xO$ (x = 0.0, 0.1, 0.5, 0.9, and 1.0) antibacterial nanoparticles loaded into basil seed mucilage (BSM)/hydrogel (BSM/HG) films via a casting method. The crystal phases, surface chemical composition, and antimicrobial efficacy of $Cu_{1.0-x}Ag_xO$ particles were characterized using X-ray diffraction (XRD), X-ray photoemission spectroscopy (XPS), and agar well diffusion assays. XRD analysis confirmed that $Cu_{1.0-x}Ag_xO$ (x = 0.1 – 0.7) samples formed composites containing CuO, Ag, and Ag_2O phases. Among them, $Cu_{0.7}Ag_{0.3}O$ exhibited superior antibacterial activity, achieving inhibition zone diameters of 8 – 13 mm against *Bacillus cereus*, *Staphylococcus aureus*, *Streptococcus thermophilus*, and *Escherichia coli*. The hydrogel demonstrated good swelling capacity and mechanical strength suitable for wound dressing applications. The incorporation of $Cu_{0.7}Ag_{0.3}O$ nanoparticles into BSM/HG films reduced both swelling capacity and tensile strength due to particle agglomeration, although the antibacterial properties were significantly enhanced. This research highlights the potential of $Cu_{1.0-x}Ag_xO$-loaded BSM/HG films for advanced wound dressing applications.

Keywords: Alginate, Antibacterial activity, Basil seed mucilage, Composite material, Copper-silver oxide, Gelatin, Hydrogel film

Introduction

Hydrogels are highly hydrated materials composed of hydrophilic polymers with networks of chemical and/or physical crosslinks between macromolecular chains [1,2]. They are used in various fields, including sensors, biomaterials, drug delivery, water treatment, tissue engineering, and soft electronics [3-7]. In wound care, hydrogels offer several advantages: they absorb exudates, maintain a moist environment, are easy to remove, and are biocompatible and safe [1,2].

Several benchmark studies have demonstrated the potential of hydrogel-based wound dressings to enhance healing rates, reduce infection, and promote tissue regeneration [8,9]. Recent advances have explored the

integration of cell-derived conditioned media (CM) into hydrogel matrices, demonstrating enhanced angiogenesis and accelerated wound repair [8]. Additionally, the development of biopolymer-based smart hydrogels that respond to wound-specific stimuli has shown significant potential in overcoming limitations of traditional dressings [9]. Hydrogels can be synthesized from natural, synthetic, or hybrid polymers [10,11]. Natural polymers like alginate, gelatin, collagen, and chitosan are commonly used, while synthetic polymers include PEG, PEO, PVA, and polypeptides. However, their weak mechanical strength limits traditional hydrogel applications [12].To address this, recent developments include dual cross-linked, double network, and topological hydrogels [13,14]. Tougher hydrogels based on cellulose, chitosan, alginate, and gelatin have been explored [15]. Gelatin (G), a denatured collagen, crosslinks easily and is widely used for its biocompatibility and biodegradability. Sodium alginate (SA) is a polyanionic copolymer that forms gels via ionic interactions with divalent or trivalent cations like Ca^{2+}, Cu^{2+}, Ba^{2+}, and Fe^{3+}. Though alginate has useful properties, it lacks biological activity and is often blended with gelatin to improve hydrogel characteristics [16]. For example, Saarai *et al.* [16] found that a 50:50 SA:G hydrogel crosslinked with Ca^{2+} offered optimal mechanical and swelling behavior. However, monovalent salts can destabilize SA-Ca^{2+} interactions. Yari *et al.* [17] enhanced SA hydrogel stability using basil seed mucilage (BSM). BSM, derived from *Ocimum basilicum L.*, contains glucomannan, xylan, and uronic acid, offering excellent water absorption [18,19]. It serves as a food stabilizer and was used here to enhance hydrogel strength and swelling [20]. Nanomaterials such as graphene oxide Jing *et al.* [21], silica Mohammed *et al.* [22], ZnO/CuO Kaptan *et al.* [23], and Ag Martinez-Higuera *et al.* [24] have also been integrated into hydrogels to boost antibacterial activity.

In this study, $Cu_{1.0-x}Ag_xO$ nanoparticles and BSM were incorporated into hydrogel films and evaluated for antibacterial activity, swelling, and mechanical performance. While several studies have incorporated metal oxide nanoparticles into biopolymer- based hydrogels for wound healing, most have focused on well- known polymers such as chitosan, alginate, or gelatin, and single oxide systems like CuO or Ag_2O. In contrast, this study introduces a novel strategy by utilizing basil seed mucilage (BSM) — a natural, underutilized, and highly swellable polysaccharide—as the hydrogel- forming matrix. Additionally, the $Cu_{1.0-x}Ag_xO$ ($0.1 \leq x \leq 0.7$) nanoparticles represent a tunable mixed metal oxide system that leverages the synergistic antibacterial properties of CuO, Ag, and Ag_2O phases within a single nanocomposite. This approach enables composition- dependent control over antibacterial efficacy and mechanical performance, distinguishing it from previous studies using simple metal oxide blends. To the best of our knowledge, the combination of BSM- based hydrogels with compositional tuning of Cu–Ag oxide nanoparticles has not yet been reported for wound dressing applications, making this study a unique contribution to the development of multifunctional hydrogel material

Materials and methods

Materials

All chemicals were of analytical grade and used without further purification. Deionized water was used throughout. $Cu_{1.0-x}Ag_xO$ (x = 0.0, 0.1, 0.5, 0.9 and 1.0) was synthesized using $Cu(NO_3)_2$, $AgNO_3$, NaOH, PEG-4000, and NH_3. Hydrogel materials included sodium alginate, gelatin, glycerol, PEG-6000, NaCl, and $CaCl_2$. Basil seeds were sourced from a local market in Udon Thani, Thailand. Antimicrobial activity was tested against *Bacillus cereus*, *Streptococcus thermophilus*, *Staphylococcus aureus*, *Escherichia coli*, *Fusarium oxysporum*, and *Penicillium* sp. The selected bacterial strains, including Gram-positive (*S. aureus*, *B. cereus*) and Gram-negative (*E. coli*, *S. thermophilus*), are clinically relevant pathogens frequently implicated in wound infections. Their inclusion allows for evaluating the broad-spectrum antibacterial potential of the hydrogel composites. Microbial strains were maintained on nutrient agar slants.

Synthesis of $Cu_{1.0-x}Ag_xO$ composite

$Cu_{1.0-x}Ag_xO$ was synthesized using a co-precipitation method modified from our previous work [25]. First, $Cu(NO_3)_2$, $AgNO_3$ and PEG-4000 were individually dissolved in DI water under constant stirring for 15 min. Next, the solution pH was adjusted to 12.0 ± 0.2 using a 1.5 M NaOH solution. Subsequently, the mixed solution was stirred vigorously

for 30 min until dark precipitates were obtained. After that, the precipitates were filtered using Whatman No. 93 filter paper and washed repeatedly with DI water. Then, the obtained particles were oven dried at 110 °C for 5 h and calcined at 600 °C for 4 h. For simplification, $Cu_{1.0-x}Ag_xO$ where x = 0.0, 0.1, 0.3, 0.5, 0.7 and 0.9 are referenced as $Cu_{1.0}O$, $Cu_{0.9}Ag_{0.1}O$, $Cu_{0.7}Ag_{0.3}O$, $Cu_{0.5}Ag_{0.5}O$, $Cu_{0.3}Ag_{0.7}O$ and $Cu_{0.1}Ag_{0.9}O$, respectively. XRD, XPS and antimicrobial activities of the nanocomposites were further investigated. The term "CuAgO" is used solely as a general abbreviation when referring to the composite group. The highest antimicrobial activity from $Cu_{1.0-x}Ag_xO$ ($Cu_{0.7}Ag_{0.3}O$), was used in fabrication of a $Cu_{0.7}Ag_{0.3}O$-loaded hydrogel film.

Preparation of BSM from basil seeds

BSM was prepared using a hydration method. First, 10 g of basil seeds were soaked in 300 mL of DI water at 40 °C for 1 h. Next, the swollen seeds were broken in a blender for 1 min and then filtered using cheese cloth. After that, the mucilage was centrifuged at 5000 rpm for 5 min to remove seed residues. Then, the BSM mucilage was oven dried at 50 °C for 24 h. Finally, brown particles of BSM were obtained and kept in a desiccator.

Preparation of BSM/HG and $Cu_{0.7}Ag_{0.3}O$-loaded BSM/HG

Hydrogel films with BSM concentrations of 0.0 – 0.9 %w/v were prepared following Saarai *et al.* [16] with slight modifications. Dried BSM was soaked in 200 mL DI water at 80 °C. Alginate (2.0% w/v), gelatin (2.0 %w/v), glycerol (2.0 %w/v), PEG-6000 (1.0 %w/v), and NaCl (0.2% w/v) were added and stirred for 30 min. The gel was cast onto a 25.4×25.4×0.2 cm aluminum plate and dried for 1 h. A 5.0 %w/v $CaCl_2$ solution was added for 15 min. Films were washed and labeled as HG, 0.1BSM/HG to 0.9BSM/HG. Mechanical and swelling properties were evaluated.

$Cu_{0.7}Ag_{0.3}O$ loaded BSM/HG was prepared in a manner similar to BSM/HG. $Cu_{0.7}Ag_{0.3}O$ particles with concentrations of 3.75, 7.50 and 15.0 mg/mL were added to the 0.5 %w/v BSM solution. Then, alginate, gelatin, glycerol, PEG-6000 and NaCl were added to the mixture. Hydrogel films with different concentrations (0.00, 3.75, 7.50 and 15.0 mg/mL) of $Cu_{0.7}Ag_{0.3}O$ are referenced as BSM/HG, 3.75$Cu_{0.7}Ag_{0.3}O$/BSM/HG, 7.50$Cu_{0.7}Ag_{0.3}O$/BSM/HG and 15.0$Cu_{0.7}Ag_{0.3}O$/BSM/HG, respectively.

Characterization techniques

The crystal structure of CuAgO particles was analyzed by X-ray diffraction (XRD, Bruker D8 Advance) using Cu Kα radiation (λ = 1.54184 Å), a 2θ range of 20° – 80°, 40 mA current, and 40 kV voltage. The chemical surface composition was examined by X-ray photoemission spectroscopy (XPS, Kratos Axis Ultra DLD) with monochromatic Al Kα radiation (10 mA, 35 kV) under a chamber pressure of 3×10^{-9} Torr. The C 1s peak at 285.0 eV was used for calibration, and Cu 2p, Ag 3d, and O 1s peaks were analyzed using a Lorentzian-Gaussian function. Functional groups of $Cu_{0.7}Ag_{0.3}O$/BSM/HG were identified via attenuated total reflectance Fourier-transform infrared spectroscopy (ATR/FT-IR, Spectrum 2, PerkinElmer) in the 4000 – 500 cm^{-1} range at 4 cm^{-1} resolution. Surface morphology and elemental composition were observed using SEM-EDX (Hitachi S 3000N, 5 kV). Films were gold-coated with a K500X sputter coater (20 mA, 5 min, 9×10^{-2} mbar) before SEM analysis.

Swelling tests

To determine the degree of swelling of the film samples, pre-weighed dried 1.0×1.0 cm film samples (W_1) were immersed in phosphate buffer (pH 7.4) at room temperature. The swollen films were removed after various immersion times, wiped with tissue paper to remove excess surface fluid and weighed (W_2). The percentage swelling ratio (SR, %) was computed after each time as follows:

$$SR\ (\%) = \frac{W_2 - W_1}{W_1} \times 100 \quad (1)$$

Tensile properties

Tensile strength and elongation at break of BSM/ HG films were measured using a Universal Testing Machine (GT- K01- GESTER) according to SATRA TM5 and ISO 20344 standard. Film strips (1. 5×10. 0 cm) were tested at a crosshead speed of

20 mm/min using a 50 mm gauge length and 5 kN load cell. All measurements were performed in 5 replicates (n = 5), and the results are reported as mean ± standard deviation.

Antimicrobial activity

The antibacterial and antifungal activities of CuAgO composites were evaluated using the agar well diffusion method. Bacterial strains (*Bacillus cereus*, *Staphylococcus aureus*, *Streptococcus thermophilus*, and *Escherichia coli*) were cultured in Mueller-Hinton broth (MHB) for 18 h at 37 °C with a 0.5 McFarland standard turbidity. Then, 100 µL of each suspension was spread on MHB agar plates. Wells (6 mm diameter) were created using a sterile cork borer, and 30 µL of CuAgO was added to each. Plates were incubated at 37 °C for 24 h. Tetracycline (50 µg) and dimethyl sulfoxide (DMSO) served as positive and negative controls. Inhibition zones were measured with a micrometer. Antifungal activity against *Fusarium oxysporum* and *Penicillium sp*. was tested similarly, using nystatin as a positive control. Antibacterial activity of BSM/HG and $Cu_{0.7}Ag_{0.3}O$/BSM/HG films was tested by disc diffusion. Films (6 mm) and filter paper discs were placed on agar plates and incubated at 37 °C for 24 h.

All experiments for swelling tests and antibacterial activity were conducted in triplicate (n = 3). Results are presented as mean ± standard deviation. Statistical analysis was performed using one-way ANOVA to assess differences between groups.

Determination of minimum inhibition concentration (MIC)

The minimum inhibitory concentration (MIC) is defined as the lowest concentration of a substance that completely inhibits visible bacterial growth after incubation at 37 °C for 24 h. In this study, the MIC values of $Cu_{0.5}Ag_{0.5}O$ and $Cu_{0.7}Ag_{0.3}O$ against *Staphylococcus aureus*, *Bacillus cereus*, and *Escherichia coli* using a broth dilution method based on the protocol described by Kamonwannasit *et al.* [26]. Bacterial suspensions were prepared at a concentration of 1×10^7 CFU/mL in Mueller-Hinton Broth (MHB). CuAgO samples were serially diluted to obtain a range of concentrations from 0.47 to 30.00 mg/L. The inoculated tubes was incubated at 37 °C for 24 h, and the MIC was recorded as the lowest concentration showing no visible bacterial growth. All experiments were conducted in triplicate to ensure reproducibility and accuracy of the results.

Results and discussion

XRD and XPS analysis

The crystal structure of CuAgO samples with different compositions calcined at 600 °C for 4 h is shown in **Figure 1**. The XRD patterns and their corresponding lattice planes of CuO in a $Cu_{1.0}O$ sample were observed at 2θ = 35.78° (−111), 38.89° (111), 48.92° (−202), 53.69° (020), 58.46° (202), 61.68° (−113), 66.47° (022), 68.37° (220), 72.79° (311) and 75.41° (004) (JCPDS No. 45-0937). This indicates a typical CuO monoclinic structure within the C*2/c* space group. CuO, Ag and Ag_2O phases were detected in $Cu_{1.0-x}Ag_xO$ (x = 0.1 - 0.7) samples. This indicates that a CuAgO composite was formed. An Ag_2O phase was observed at 2θ = 38.40° (011) that corresponds to the hexagonal structure of silver oxide within the P*3m1* space group (JCPDS No. 72-2108). Metallic Ag was also found at 2θ = 38.40° (111), 44.63° (200), 64.79° (220) and 77.56° (311), which implies the presence of the face centered cubic crystalline structure of silver within the F*m3m* space group (JCPDS No. 04-0783). Detection of a CuO phase was impossible due to the very small fraction of copper in $Cu_{0.1}Ag_{0.9}O$ samples.

XPS analysis was conducted to confirm the XRD results. This technique is normally used to identify the elements present on the surface of a specimen, as well as the valence states and interactions of each atom. **Figure 2** displays the XPS spectra of O 1s, Cu 2p and Ag 3d core levels from the $Cu_{0.7}Ag_{0.3}O$ sample. In Cu 2p spectra (**Figure 2(a)**), characteristic double peaks at 952.72 and 932.93 eV correspond to Cu $2p_{1/2}$ and Cu $2p_{3/2}$, respectively. The 19.8 eV energy gap between these levels is due to spin-orbit coupling and is in good agreement with the literature values [27-30]. Additionally, 2 bands at 942.46 and 961.02 eV can be ascribed to the shake-up satellite peaks of Cu^{2+} in CuO with d^9 configuration in its ground state. Therefore, the appearance of the satellite peaks indicates the presence of the CuO species in the surface layer.

The XPS spectrum of Ag 3d (**Figure 2(b)**) reveals 2 peaks at 373.87 and 367.99 eV with an energy gap of

5.88 eV (spin-orbit splitting) indicating Ag $3d_{3/2}$ and Ag $3d_{5/2}$, respectively. This suggests formation of metallic silver (Ag^0) in the composite. Moreover, the Ag $3d_{3/2}$ and Ag $3d_{5/2}$ core levels shift towards lower binding energies, 373.01 and 367.29 eV, respectively. This is due to the presence of silver ions in Ag_2O (Ag^+), in agreement with the literature [31,32]. The presence of ~53 % metallic Ag relative to the amount of Ag_2O is also in agreement with XRD results. The XPS spectrum of O 1s (**Figure 2(c)**) shows 3 peaks at 529.23, 531.67 and 533.14 eV. The peak centered at 529.23 eV corresponds to the O 1s of Cu–O or Ag–O in the form of CuO and Ag_2O. The peaks at 531.67 and 533.14 eV correspond to oxygen adsorbed on the composite surface [28,32].

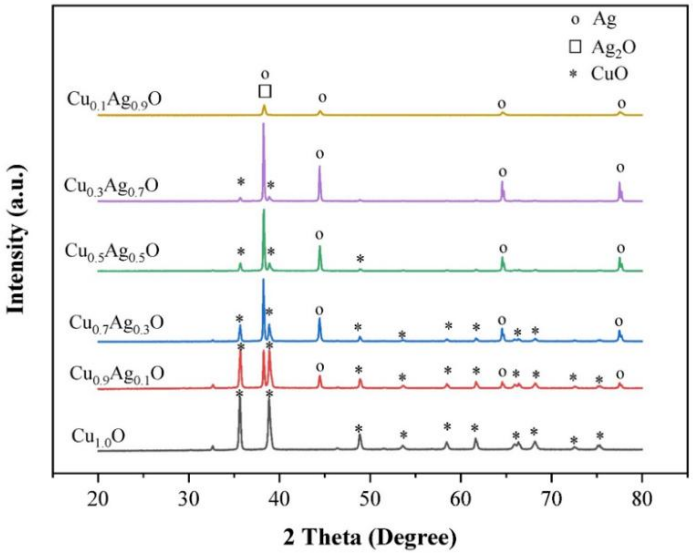

Figure 1 XRD patterns of CuAgO composites calcined at 600 °C for 4 h.

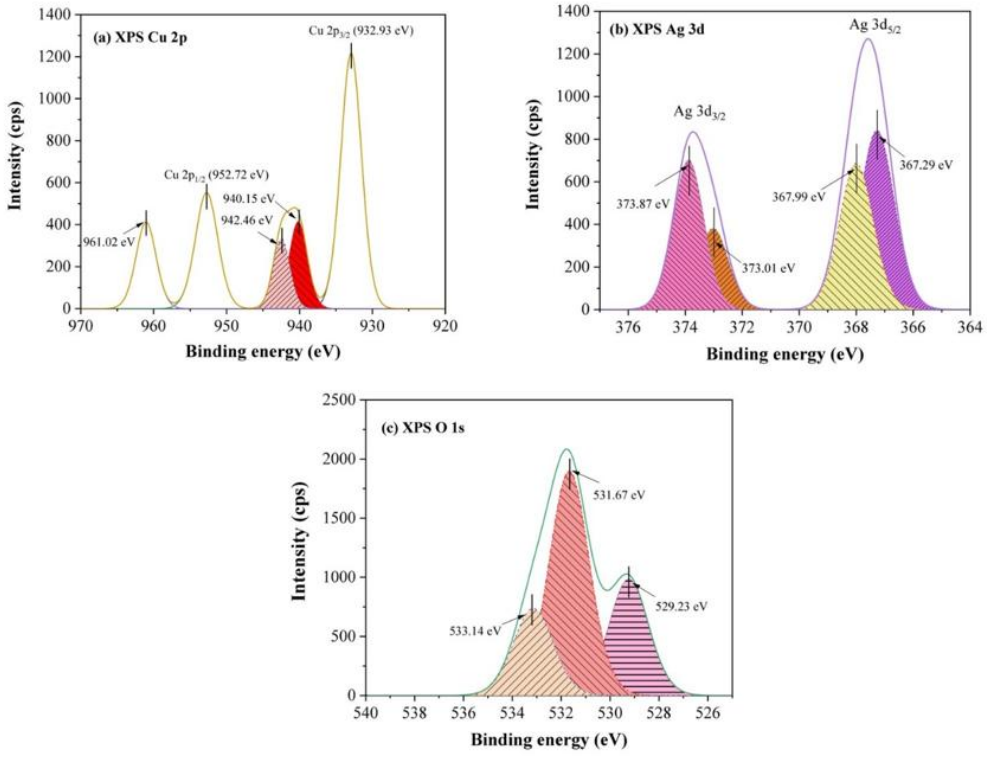

Figure 2 (a) Cu 2p, (b) Ag 3d and (c) O 1s XPS spectra of $Cu_{0.7}Ag_{0.3}O$ composite calcined at 600 °C for 4 h.

Antimicrobial activity of CuAgO composites

The antibacterial activity of CuAgO at a concentration of 30 mg/mL against 4 bacterial strains was evaluated using an agar well diffusion technique. **Table 1** shows the inhibition diameter around wells with CuAgO particles against bacterial strains after 24 h of incubation. A larger diameter of inhibition indicates greater antibacterial activity. As expected, the DMSO negative control was ineffective against all bacterial strains, while tetracycline (50 μg/mL), a positive control, was effective with inhibition diameters of 11 – 29 mm. No strains were inhibited by the $Cu_{1.0}O$ sample at a 30 mg/mL concentration. Inhibition zones of $Cu_{0.3}Ag_{0.7}O$, $Cu_{0.5}Ag_{0.5}O$, $Cu_{0.7}Ag_{0.3}O$ and $Cu_{0.9}Ag_{0.1}O$ samples developed inhibition widths ranging from 8 – 13 mm for all bacterial strains. Moreover, the Gram-negative bacterial strain, *Escherichia coli*, was only affected by the $Cu_{0.1}Ag_{0.9}O$ sample with an inhibition diameter of 7.0 mm. These results show that Gram-positive and Gram-negative bacteria had similar susceptibility.

MIC, a parameter indicating inhibitory efficacy, refers to the lowest concentration of an antibacterial reagent that will prevent bacterial growth after 24 h of incubation. $Cu_{0.5}Ag_{0.5}O$ and $Cu_{0.7}Ag_{0.3}O$ samples were chosen to determine the MIC values against *Staphylococcus aureus, Bacillus cereus* and *Escherichia coli*. The results are shown in **Table 2**. A MIC of 3.75 mg/mL against *Escherichia coli* was obtained for the $Cu_{0.7}Ag_{0.3}O$ sample, while higher MIC values were observed against *Bacillus cereus* (7.5 mg/mL) and *Staphylococcus aureus* (15.0 mg/mL). For the $Cu_{0.5}Ag_{0.5}O$ sample, the lowest MIC value, 0.94 mg/mL, was obtained against *Bacillus cereus*, while a MIC value of 15 mg/mL was found against *Escherichia coli* and *Staphylococcus aureus*. The present study revealed that the $Cu_{0.7}Ag_{0.3}O$ sample had the optimal Cu:Ag molar ratio, 0.7:0.3, for antibacterial activity. This composition was used in subsequent fabrication of $Cu_{0.7}Ag_{0.3}O$/BSM/HG films. Moreover, antifungal activities of all CuAgO composites were investigated against *Fusarium oxysporum* and *Penicillium sp.* These results are shown in **Table 1**. Nystatin (50 μg/mL) was effective against *Fusarium oxysporum* and *Penicillium sp.* with inhibition zones of 2.30 and 1.50 mm, respectively. No CuAgO samples were effective against any of the fungal strains tested at 30 mg/mL.

Swelling properties of BSM/HG film

The swelling ratio of hydrogel films is used for measuring their fluid absorbing capacities, which is particularly useful for wound dressing materials. These results are shown in **Figure 3**. The swelling ratio of HG and 0.1BSM/HG increased gradually with time (**Figure 3(A)**). For 0.3BSM/HG and 0.5BSM/HG samples, the swelling ratio of the film increased sharply until 120 min of immersion in a buffer solution, and then started to decrease. The decreased swelling ratio is due to dissolution of alginate in the aqueous medium. Extension of the SA chains causes breakdown of the crosslinking bonds in the presence of phosphate anion in the buffer [33]. Thus, a portion of SA may dissolve in PBS medium, resulting in a decreased polymer mass. For 0.7BSM/HG and 0.9BSM/HG samples, the swelling ratio of the films showed similar trends where it rises quickly in the first 90 min, and then slowly increased until 240 min of immersion. After 120 min of immersion (**Figure 3(B)**), neat HG films exhibited a swelling ratio of 1442 %. Greater BSM filler, up to 0.5 %w/v, increased the film swelling ratio. The 0.5BSM/HG specimen exhibited a 2102 % maximal swelling ratio. Notably, this was higher than that of a commercial sodium alginate hydrogel film (50 – 1800 %) [34]. Among the tested films, the 0.7BSM/HG and 0.9BSM/HG films showed low swelling ratios, which was presumably due to agglomeration of BSM particles.

Tensile properties of BSM/HG films

Generally, hydrogel films used as wound dressings need better mechanical properties because the wound surface will change with body movements. The mechanical properties of HG and BSM/HG films are shown in **Figure 4**.

Table 1 Antimicrobial activities of synthesized CuAgO samples against 4 different bacterial and fungal strains.

Type of bacteria/Fungi	Inhibition diameter (mm) (30 mg/mL)	Tetracycline (50 μg/mL)	Nystatin (50 μg/mL)
$Cu_{0.9}Ag_{0.1}O$			
Bacillus cereus	9.00 ± 1.40	–	–
Staphylococcus aureus	12.00 ± 0.00	–	–
Streptococcus thermophilus	10.30 ± 0.60	–	–
Escherichia coli	9.30 ± 1.20	–	–
Fusarium oxysporum	ND	–	–
Penicillium sp.	ND	–	–
$Cu_{0.7}Ag_{0.3}O$			
Bacillus cereus	8.50 ± 0.70	–	–
Staphylococcus aureus	12.70 ± 3.20	–	–
Streptococcus thermophilus	11.00 ± 1.00	–	–
Escherichia coli	9.70 ± 0.60	–	–
Fusarium oxysporum	ND	–	–
Penicillium sp.	ND	–	–
$Cu_{0.5}Ag_{0.5}O$			
Bacillus cereus	10.00 ± 0.00	–	–
Staphylococcus aureus	8.30 ± 0.60	–	–
Streptococcus thermophilus	11.30 ± 0.60	–	–
Escherichia coli	9.70 ± 0.60	–	–
Fusarium oxysporum	ND	–	–
Penicillium sp.	ND	–	–
$Cu_{0.3}Ag_{0.7}O$			
Bacillus cereus	9.00 ± 0.00	–	–
Staphylococcus aureus	9.00 ± 0.00	–	–
Streptococcus thermophilus	*	–	–
Escherichia coli	8.00 ± 0.00	–	–
Fusarium oxysporum	ND	–	–
Penicillium sp.	ND	–	–
$Cu_{0.1}Ag_{0.9}O$			
Bacillus cereus	ND	–	–
Staphylococcus aureus	ND	–	–
Streptococcus thermophilus	*	–	–
Escherichia coli	7.00 ± 0.00	–	–
Fusarium oxysporum	ND	–	–
Penicillium sp.	ND	–	–
$Cu_{1.0}O$			
Bacillus cereus	ND	–	–
Staphylococcus aureus	ND	–	–
Streptococcus thermophilus	ND	–	–
Escherichia coli	ND	–	–
Fusarium oxysporum	ND	–	–
Penicillium sp.	ND	–	–
Tetracycline			
Bacillus cereus	–	17.70 ± 0.60	–
Staphylococcus aureus	–	28.30 ± 5.70	–

Type of bacteria/Fungi	Inhibition diameter (mm) (30 mg/mL)	Tetracycline (50 μg/mL)	Nystatin (50 μg/mL)
Streptococcus thermophilus	–	11.00 ± 1.00	–
Escherichia coli	–	18.00 ± 1.00	–
Nystatin			
Fusarium oxysporum	–	–	2.30 ± 0.10
Penicillium sp.	–	–	1.50 ± 0.00
ND = not detected; * not tested			

Table 2 MIC of $Cu_{0.5}Ag_{0.5}O$ and $Cu_{0.7}Ag_{0.3}O$ against *Bacillus cereus*, *Staphylococcus aureus* and *Escherichia coli*.

Type of bacteria	MIC (mg/mL)	
	$Cu_{0.7}Ag_{0.3}O$	$Cu_{0.5}Ag_{0.5}O$
Bacillus cereus	7.50	0.94
Staphylococcus aureus	15.0	15.0
Escherichia coli	3.75	15.0

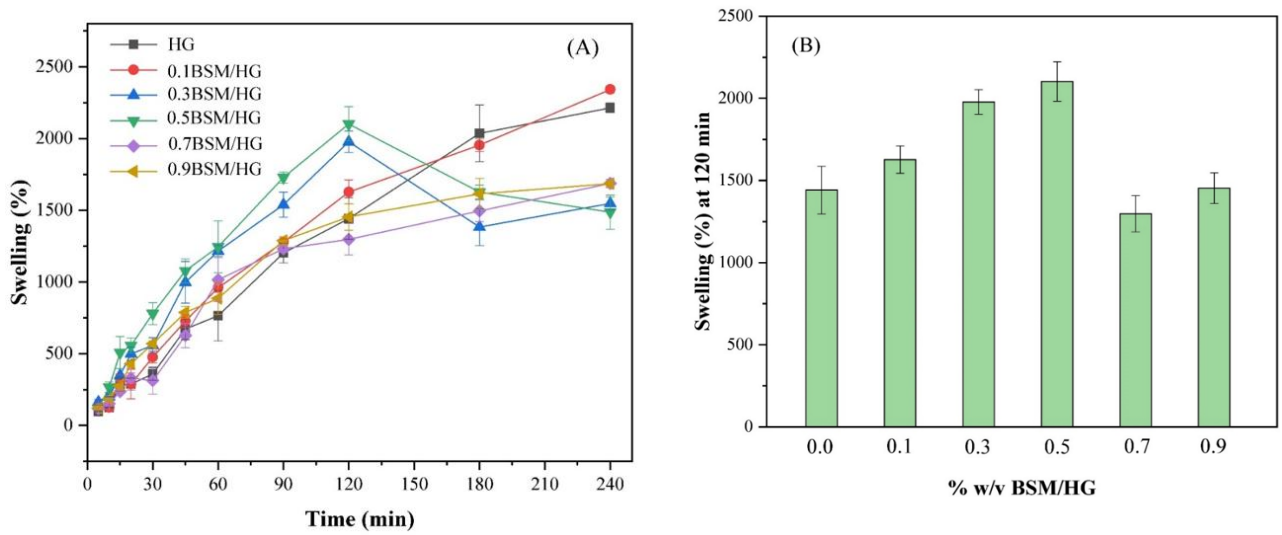

Figure 3 Swelling properties of HG, 0.1BSM/HG, 0.3BSM/HG, 0.5BSM/HG, 0.7BSM/HG and 0.9BSM/HG.

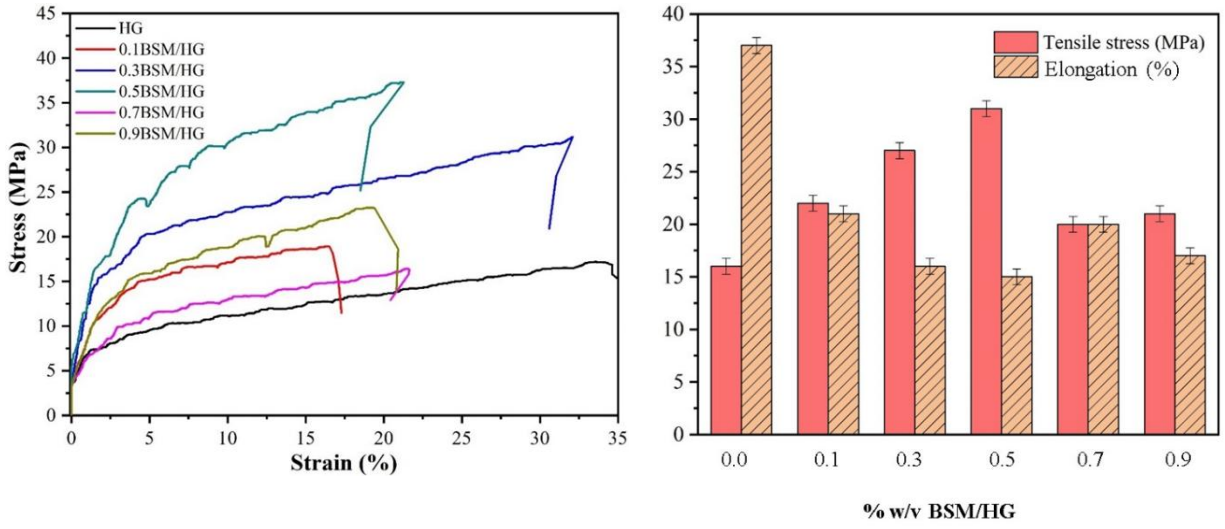

Figure 4 Tensile properties of HG, 0.1BSM/HG, 0.3BSM/HG, 0.5BSM/HG, 0.7BSM/HG and 0.9BSM/HG.

Stress-at-break and elongation-at-break of pure HG film were 16 MPa and 37%, respectively. The tensile stress of BSM/HG films increased with BSM content up to 0.5% w/v BSM (31 MPa), and then decreased with increasing amounts of BSM. Dispersion of BSM particles in the HG is important since uniformly dispersed BSM enhances the mechanical properties of a hydrogel. However, additional increases in BSM content cause formation of excessive numbers of BSM particles and subsequent accumulation. Moreover, the elongation-at-break of BSM/HG tended to decrease relative to the amount of BSM present, related to increased tensile stress. Since the 0.5BSM/HG film sample gave better swelling and mechanical properties than other samples, it was used for incorporation with $Cu_{0.7}Ag_{0.3}O$ particles, which showed the highest antibacterial activity.

SEM-EDX and FT-IR analysis of $Cu_{0.7}Ag_{0.3}O$/BSM/HG films

SEM images of BSM/HG and 7.5$Cu_{0.7}Ag_{0.3}O$/BSM/HG films with a 5000× magnification are presented in **Figure 5**. The morphology of the pure HG film was rough with a non-porous structure (**Figure 5(a)**). For BSM/HG films with various concentrations of BSM, film roughness increases with BSM content (**Figures 5(b)** - **(d)**), particularly in 0.7BSM/HG (**Figure 5(c)**) and 0.9BSM/HG (**Figure 5(f)**) samples. This could be due to agglomeration of BSM particles. The 0.5BSM/HG film sample seems to have the best composition with smooth and non-porous surfaces, indicating a good distribution of BSM particles in the hydrogel matrix. Moreover, SEM imagery of the $Cu_{0.7}Ag_{0.3}O$/BSM/HG film (**Figure 5(g)**) showed rough and non-porous surfaces. However, $Cu_{0.7}Ag_{0.3}O$ particles were not observed using this technique.

Elemental distribution of Ag and Cu in the 7.5 $Cu_{0.7}Ag_{0.3}O$/BSM/HG film was analyzed using EDS mapping. These results are shown in **Figure 6**, where Cu and Ag particles in the hydrogel matrix were homogeneously distributed. Moreover, the major constituents of 7.5 $Cu_{0.7}Ag_{0.3}O$ loaded BSM/HG films were C, O, Cl and Ca. The presence of C may be due to the carbon tape used on the SEM stub during analysis as well as substances incorporated in the hydrogel films (PEG, sodium alginate, gelatin, BSM). Trace amounts of Na in the samples are due to NaCl used in the preparation of hydrogel film. Trace amounts of Cu and Ag were also detected.

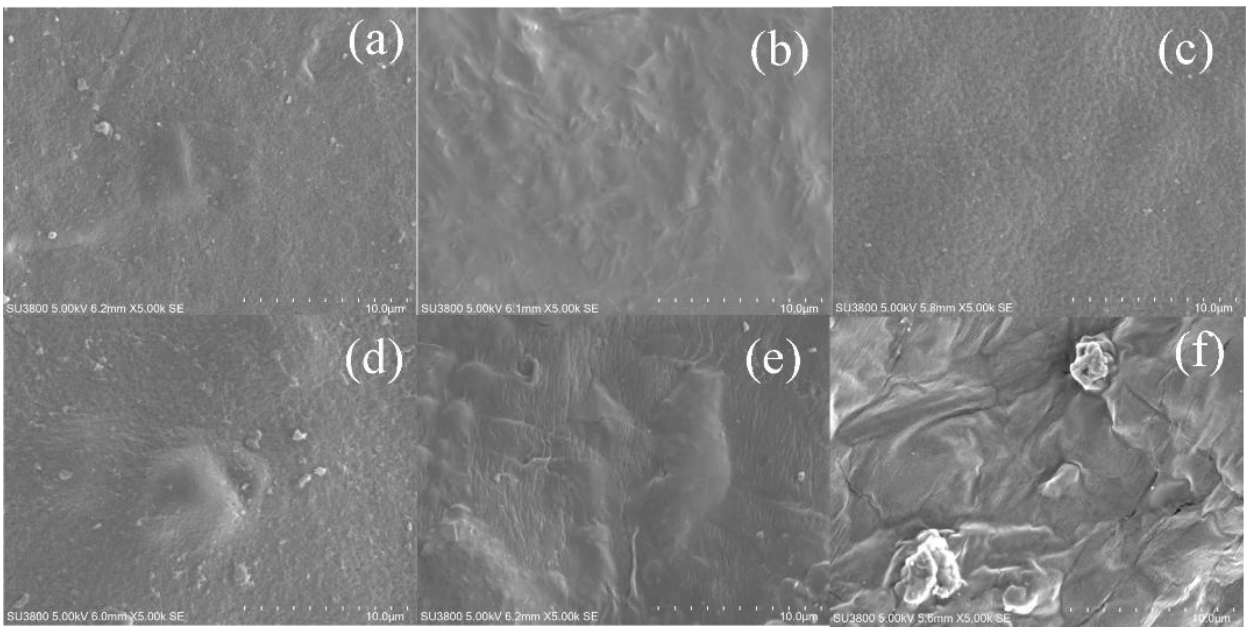

Figure 5 SEM imagery of (a) HG, (b) 0.1BSM/HG, (c) 0.5BSM/HG, (d) 0.7BSM/HG, (e) 0.9BSM/HG and (f) 7.5 $Cu_{0.7}Ag_{0.3}O$/BSM/HG.

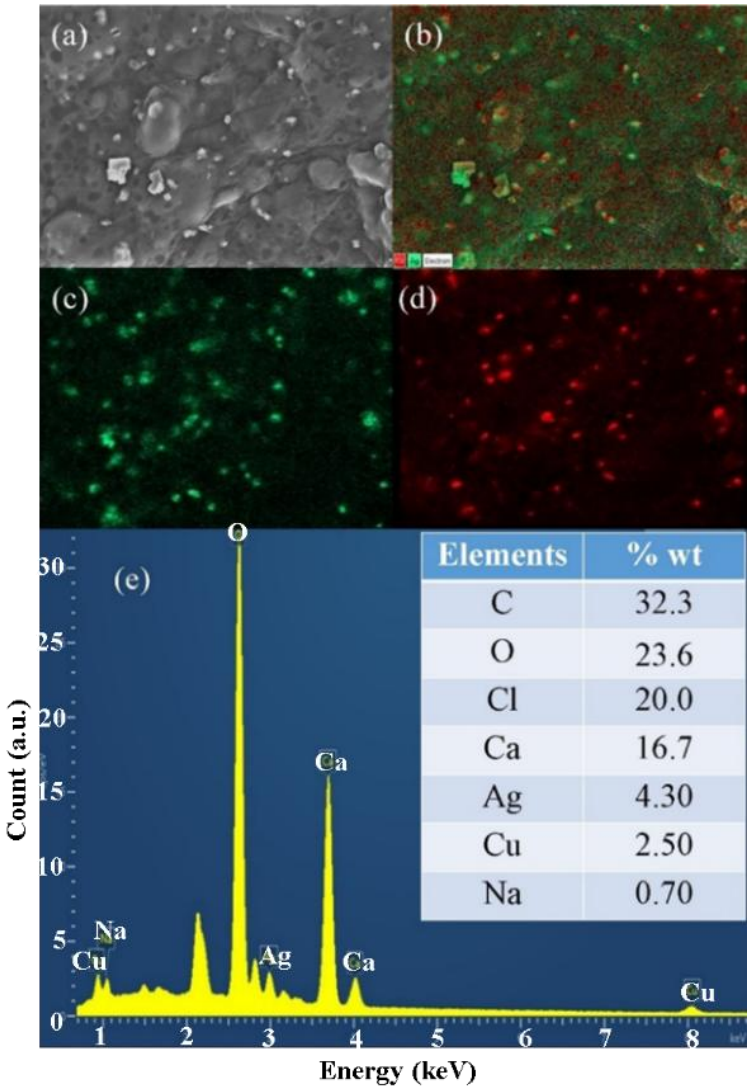

Figure 6 EDS mapping displays distribution of Ag and Cu elements in 7.5 $Cu_{0.7}Ag_{0.3}O$/BSM/HG: (a) secondary electron image, (b) the element sensitive map of combined Cu and Ag, (c) the element sensitive map of Ag, (d) the element sensitive map of Cu, and (e) EDS spectrum of 7.5$Cu_{0.7}Ag_{0.3}O$/BSM/HG

Figure 7 shows the FT-IR spectra of a $Cu_{0.7}Ag_{0.3}O$/BSM/HG film. The peaks of all samples are less distinct. The broad peaks between ~3000 and 3600 cm^{-1}, and 1626 cm^{-1} correspond to stretching and bending vibrations of the hydroxyl (OH^-) groups of alginate, gelatin, BSM and PEG. The small peak at 2915 cm^{-1} is attributed to C–H stretching. Peaks at 1640 and 1539 cm^{-1} can be ascribed to the C=O and C–N stretching vibration of gelatin. Bands at 1640, 1435 and 1038 cm^{-1} indicate C–OO asymmetric stretching vibrations of free carboxylate, C–OO symmetric stretching, and C–O–C stretching of BSM and alginate, respectively [18,35].

Swelling and tensile properties of $Cu_{0.7}Ag_{0.3}O$/BSM/HG films

The swelling ratio of the $Cu_{0.7}Ag_{0.3}O$/BSM/HG film is shown in **Figure 8(A)**. The swelling ratio of BSM/HG was 2102 %. In $Cu_{0.7}Ag_{0.3}O$ loaded HG, the swelling ratios of all samples decreased approximately fourfold compared to that of BSM/HG. This decreased swelling capacity is presumably due to weakened mechanical interactions between the $Cu_{0.7}Ag_{0.3}O$ particles and the hydrogel matrix, as well as nanoparticle agglomeration. $Cu_{0.7}Ag_{0.3}O$ particles can occupy the mesh space or pore volume within the gel network, thereby hindering diffusion and penetration into the matrix [36]. Although high-resolution SEM or image-based analysis was not performed in this work,

similar observations and interpretations have been reported in previous studies [36,37].

Tensile strength and elongation of $Cu_{0.7}Ag_{0.3}O$ loaded BSM/HG are present in **Figure 8(B)**. The tensile stress and elongation of BSM/HG were 31 MPa and 16 %, respectively. In $Cu_{0.7}Ag_{0.3}O$ loaded BSM/HG, tensile stress and elongation were clearly low. These decreased swelling and mechanical properties of $Cu_{0.7}Ag_{0.3}O$ loaded BSM/HG could be due to agglomeration and increased inhomogeneity of $Cu_{0.7}Ag_{0.3}O$ particles. Lack of interfacial adhesion between the polymer matrix and oxide particles caused decreased tensile strength and swelling capacity [38].

Antibacterial activity of $Cu_{0.7}Ag_{0.3}O$-loaded BSM/HG films

The antibacterial activities of $Cu_{0.7}Ag_{0.3}O$ (3.75, 7.50 and 15.0 mg/mL) loaded BSM/HG films against *Staphylococcus aureus* and *Bacillus cereus* were investigated using a disc diffusion method. These results are shown in **Figure 9** and **Table 3**.

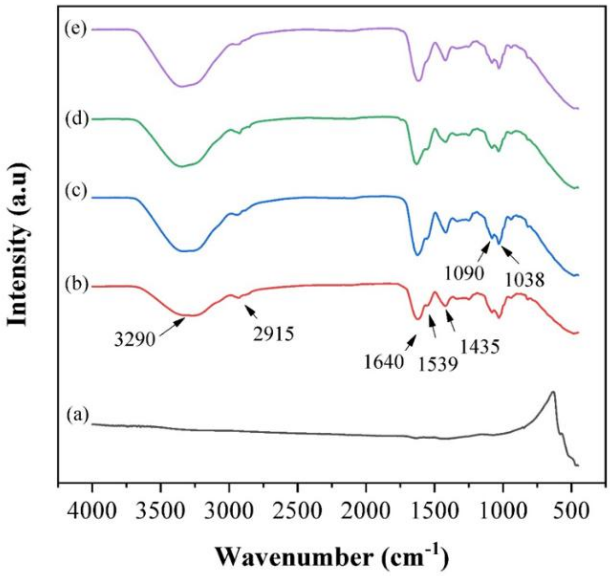

Figure 7 FT-IR spectra of (a) $Cu_{0.7}Ag_{0.3}O$, (b) 0.5BSM/HG, (c) 3.75$Cu_{0.7}Ag_{0.3}O$/BSM/HG, (d) 7.50$Cu_{0.7}Ag_{0.3}O$/BSM/HG and (e) 15.0$Cu_{0.7}Ag_{0.3}O$/BSM/HG.

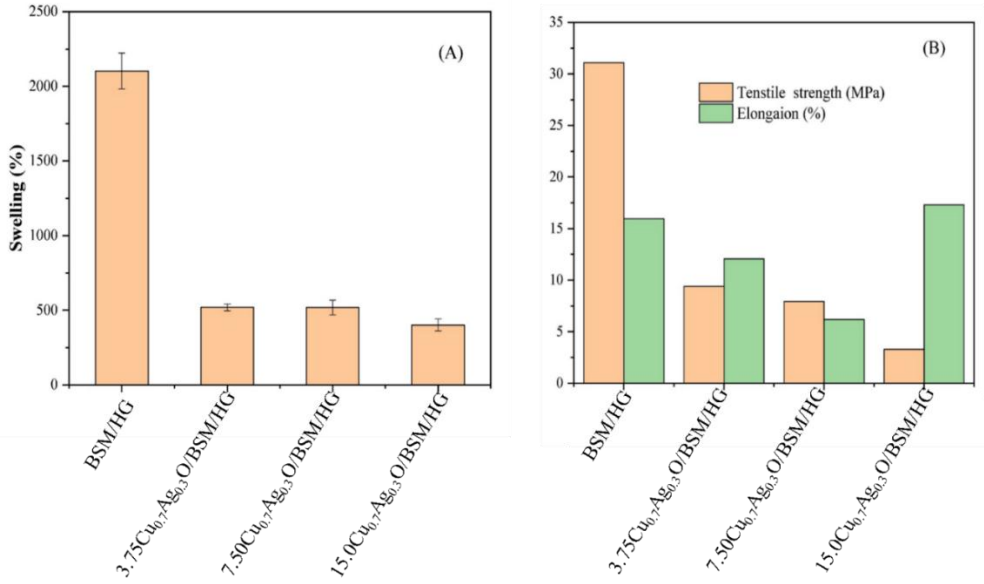

Figure 8 (A) Swelling, and (B) tensile properties of $Cu_{0.7}Ag_{0.3}O$/BSM/HG.

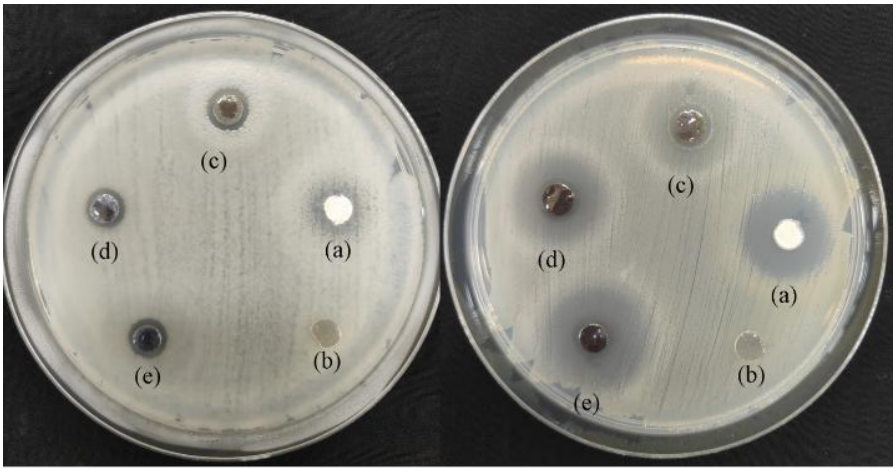

Figure 9 Imagery of the antibacterial activity of $Cu_{0.7}Ag_{0.3}O$/BSM/HG against *Bacillus cereus* and *Staphylococcus aureus*: (a) Positive control, (b) BSM/HG, (c) 3.75$Cu_{0.7}Ag_{0.3}O$/BSM/HG, (d) 7.50$Cu_{0.7}Ag_{0.3}O$/BSM/HG and (e) 15.0 $Cu_{0.7}Ag_{0.3}O$/BSM/HG.

Table 3 Antibacterial activity of $Cu_{0.7}Ag_{0.3}O$/BSM/HG samples against *Bacillus cereus* and *Staphylococcus aureus*.

Type of bacteria	Inhibition diameter (mm)	Tetracycline (50 μg/mL)
3.75$Cu_{0.7}Ag_{0.3}O$/BSM/HG		
Bacillus cereus	9.33 ± 0.06	–
Staphylococcus aureus	18.00 ± 0.00	–
7.50$Cu_{0.7}Ag_{0.3}O$/BSM/HG		
Bacillus cereus	8.67 ± 0.06	–
Staphylococcus aureus	18.00 ± 0.00	–
15.0$Cu_{0.7}Ag_{0.3}O$/BSM/HG		
Bacillus cereus	8.33 ± 1.00	–
Staphylococcus aureus	20.33 ± 0.15	–
Tetracycline		
Bacillus cereus	–	9.33 ± 0.12
Staphylococcus aureus	–	18.67 ± 0.06

Figure 9 and **Table 3** show the width of inhibition zone around discs with $Cu_{0.7}Ag_{0.3}O$/BSM/HG samples against bacterial strains after incubation for 24 h. There were no inhibition zones detected for BSM/HG films against *Bacillus cereus* and *Staphylococcus aureus*, whereas the tetracycline positive control was effective at 50 μg/mL with inhibition zones of 9 –19 mm. All $Cu_{0.7}Ag_{0.3}O$/BSM/HG samples showed effective antibacterial activities against all tested strains with inhibition widths ranging from 8 – 21 mm. Larger inhibition zones, 18 – 21 mm, were observed for *Staphylococcus aureus*, indicating that this bacterium was more sensitive than *Bacillus cereus*. Moreover, the 3.75 $Cu_{0.7}Ag_{0.3}O$/BSM/HG sample had the best performance, providing effective antibacterial activity with the lowest concentration of $Cu_{0.7}Ag_{0.3}O$. $Cu_{0.7}Ag_{0.3}O$ particles with a minimum concentration of 3.75 mg/mL in a 3.75$Cu_{0.7}Ag_{0.3}O$/BSM/HG film showed the greatest antibacterial activities against *Staphylococcus aureus* and *Bacillus cereus*.

These findings suggest that the antibacterial performance of $Cu_{0.7}Ag_{0.3}O$/BSM/HG films is

comparable to or better than some commercial hydrogel-based wound dressings containing silver or copper agents. For example, products such as Aquacel Ag and Acticoat Alobaid *et al.* [39] typically exhibit inhibition zones in the range of 10 – 20 mm against Gram-positive bacteria, similar to the 18 – 21 mm observed in this study. Moreover, the ability of the 3.75 $Cu_{0.7}Ag_{0.3}O$/BSM/HG sample to achieve these effects at low nanoparticle concentrations highlights the potential for reduced cytotoxicity and cost-effectiveness in clinical applications. These results support the feasibility of applying $Cu_{0.7}Ag_{0.3}O$/BSM/HG films as multifunctional wound dressings with enhanced antibacterial efficacy.

Although this study demonstrates promising antibacterial performance and swelling behavior of the $Cu_{0.7}Ag_{0.3}O$/BSM/HG films, cytotoxicity and biocompatibility assessments were not conducted and remain essential for clinical translation. Future work will focus on evaluating the *in vitro* and *in vivo* biocompatibility of the hydrogel films to ensure their safety and efficacy in wound healing applications.

Conclusions

This study demonstrates the successful synthesis and incorporation of $Cu_{0.7}Ag_{0.3}O$ nanoparticles into basil seed mucilage (BSM)/hydrogel (HG) films for potential biomedical applications. The $Cu_{0.7}Ag_{0.3}O$ composite exhibited the highest antibacterial activity, attributed to the synergistic effects of metallic Ag, Ag_2O, and CuO phases confirmed by XRD and XPS analyses. Incorporating $Cu_{0.7}Ag_{0.3}O$ into BSM/HG films led to a reduction in swelling capacity and tensile strength due to particle agglomeration, though the antibacterial performance against *Staphylococcus aureus* and *Bacillus cereus* remained exceptional, even at a low nanoparticle concentration of 3.75 mg/mL. The 0.5 % w/v BSM/HG film demonstrated superior mechanical and swelling properties, highlighting the critical role of BSM concentration in optimizing film performance. The uniform distribution of Ag and Cu particles within the hydrogel matrix was achieved, showcasing the effectiveness of the casting method for composite film fabrication.

This work represents a novel approach by combining a rarely studied natural biopolymer (BSM) with compositionally tunable Cu–Ag oxide nanoparticles, forming multifunctional hydrogel films with antibacterial properties not previously reported.

These findings underscore the potential of $Cu_{0.7}Ag_{0.3}O$-loaded BSM/HG films as multifunctional wound dressings with enhanced antibacterial properties. Future work should explore strategies to further improve the uniformity of particle dispersion to minimize agglomeration and maintain mechanical integrity. Additionally, investigations into the cytocompatibility and long-term stability of these films under physiological conditions will be essential for advancing their biomedical applications.

Acknowledgements

The authors would like to thank the Department of Chemistry, Faculty of Science, Udon Thani Rajabhat University (Thailand) for providing spectroscopy analysis. We also thank Professor Dr. Jeffrey C. Nash from the Office of Graduate Studies (Retired) of the Udon Thani Rajabhat University for his support in proofreading this manuscript.

Declaration of Generative AI in Scientific Writing

The authors used a generative AI tool (ChatGPT, OpenAI) solely for English grammar and language improvement. The scientific content, data interpretation, and conclusions were entirely developed by the authors.

CRediT Author Statement

Jiyapa Sripirom: Methodology, Data curation, Formal analysis, Writing- Reviewing and Editing.

Rungrudee Srisomang: Methodology, Reviewing and Editing.

Sakuntala Siri-Udom: Methodology, Reviewing and Editing.

Cybelle Morales Futalan: Methodology, Reviewing and Editing.

Khongvit Prasitnok: Methodology, Reviewing and Editing.

Orrasa Prasitnok: Methodology, Reviewing and Editing.

Sirilak Kamonwannasit: Methodology, Reviewing and Editing.

Agarat Kamcharoen: Methodology, Reviewing and Editing.

Pongtanawat Khemthong: Methodology, Reviewing and Editing.

Piaw Phatai: Conceptualization, Supervision, Writing-Reviewing and Editing, Project administration.

References

[1] V Brumberg, T Astrelina, T Malivanova and A Samoilov. Modern wound dressings: Hydrogel dressings. *Biomedicines* 2021; **9(9)**,1235.

[2] MB Labowska, K Cierluk, AM Jankowska, J Kulbacka, J Detyna and I Michalak. A review on the adaption of alginate-gelatin hydrogels for 3D cultures and bioprinting. *Materials* 2021; **14(4)**, 858.

[3] S Yue, H He, B Li and T Hou. Hydrogel as a biomaterial for bone tissue engineering: A review. *Nanomaterials* 2020; **10(8)**, 1511.

[4] H Zhang, Q Song, Z Deng, J Ren and X Xiang. Sodium alginate hydrogel toughened by guar gum for strain sensors. *Polymer Bulletin* 2024; **81**, 8045-8056.

[5] ME Batouti, W Sadik, AG Eldemerdash, E Hanafy and HA Fetouh. New and innovative microwave-assisted technology for synthesis of guar gum-grafted acrylamide hydrogel superabsorbent for the removal of acid red 8 dye from industrial wastewater. *Polymer Bulletin* 2023; **80(5)**, 4965-4989.

[6] M Moradi, A Barati, S Moradi and E Zarinabadi. Synthesis and characterization of starch-based hydrogels containing myrtus oil nanoemulsion for wound dressings. *Polymer Bulletin* 2023; **80**, 3043-3062.

[7] KGD Oznur and TDA Pınar. Statistical evaluation of biocompatibility and biodegradability of chitosan/gelatin hydrogels for wound-dressing applications. *Polymer Bulletin* 2024; **81**, 1563-1596.

[8] G Nifontova, S Safaryan, Y Khristidis, O Smirnova, M Vosough, A Shpichka and P Timashev. Advancing wound healing by hydrogel-based dressings loaded with cell-conditioned medium: A systematic review. *Stem Cell Research & Therapy* 2024; **15(1)**, 371.

[9] R Jaiswal and AP Sherje. Recent advances in biopolymer-based smart hydrogel for wound healing. *Journal of Drug Delivery Science and Technology* 2024; **99**, 105990.

[10] S Bashir, M Hina, J Iqbal, AH Rajpar, MA Mujtaba, NA Alghamdi, S Wageh, K Ramesh and S Ramesh. Fundamental concepts of hydrogels: Synthesis, properties, and their applications. *Polymers* 2020; **12(11)**, 2702.

[11] NP Esfahani, N Koupaei and H Bahreini. Fabrication and characterization of a novel hydrogel network composed of polyvinyl alcohol/polyvinylpyrrolidone/nano-rGO as wound dressing application. *Journal of Polymer Research* 2023; **30**, 56.

[12] X Lin, X Zhao, C Xu, L Wang and Y Xia. Progress in the mechanical enhancement of hydrogels: Fabrication strategies and underlying mechanisms. *Journal of Polymer Science* 2022; **60(17)**, 2525-2542.

[13] Q Chen, H Chen, L Zhu and J Zheng. Fundamentals of double network hydrogels. *Journal of Materials Chemistry B* 2015; **3(18)**, 3654-3676.

[14] KO Rojek, M Cwiklinska, J Kuczak and J Guzowski. Microfluidic formulation of topological hydrogels for microtissue engineering. *Chemical Reviews* 2021; **122(22)**, 16839-16909.

[15] S Cometa, C Licini, MA Bonifacio, P Mastrorilli, M Mattioli-Belmonte and ED Giglio. Carboxymethyl cellulose-based hydrogel film combined with berberine as an innovative tool for chronic wound management. *Carbohydrate Polymers* 2022; **283**, 119145.

[16] A Saarai, V Kasparkova, T Sedlacek and P Saha. On the development and characterisation of crosslinked sodium alginate/gelatine hydrogels. *Journal of the Mechanical Behavior of Biomedical Materials* 2013; **18**, 152-166.

[17] K Yari, I Akbari and SAV Yazdi. Development and evaluation of sodium alginate-basil seeds mucilage beads as a suitable carrier for controlled release of metformin International Journal of Biological Macromolecules 2020; **159**, 1-10.

[18] F Kurd, M Fathi and H Shekarchizadeh. Basil seed mucilage as a new source for electrospinning: Production and physicochemical characterization. *International Journal of Biological Macromolecules* 2017; **95**, 689-695.

[19] N Srikhao, K Chirochrapas, N Kwansanei, P Kasemsiri, A Ounkaew, M Okhawilai, C Likitaporn, S Theerakulpisut and H Uyama. Multi-responsive optimization of novel pH-sensitive hydrogel beads based on basil seed mucilage, alginate, and magnetic particles. *Gels* 2022; **8(5)**, 274.

[20] S Nazir and IA Wani. Functional characterization of basil (*Ocimum basilicum L.*) seed mucilage. *Bioactive Carbohydrates and Dietary Fibre* 2021; **25**, 100261.

[21] X Jing, H Mi, BN Napiwocki, X Peng and L Turng. Mussel-inspired electroactive chitosan/graphene oxide composite hydrogel with rapid self-healing and recovery behavior for tissue engineering. *Carbon* 2017; **125**, 557-570.

[22] AA Mohammed, S Li, T Sang, JR Jones and A Pinna. Nanocomposite hydrogels with polymer grafted silica nanoparticles using glucose oxidase. *Gels* 2023; **9(6)**, 486.

[23] Y Kaptan, O Karal-Yilmaz, B Izbudak, B Giray, B Yilmaz and A Bal-Ozturk. Preparation of tetracycline hydrochloride loaded chitosan/silk fibroin/ZnO antibacterial biocomposite hydrogel sponges for wound healing application. *Journal of Polymer Research* 2023; **30**, 49.

[24] A Martinez-Higuera, C Rodriguez-Beas, JMA Villalobos-Noriega, A Arizmendi-Grijalva, C Ochoa-Sanchez, E Larios-Rodriguez, JM Martinez-Soto, E Rodriguez-Leon, C Ibarra-Zazueta, R Mora-Monroy, HA Borbon-Nunez, A Garcia-Galaz, MDC Candia-Plata, LF Lopez-Soto and R Iniguez-Palomares. Hydrogel with silver nanoparticles synthesized by Mimosa tenuiflora for second-degree burns treatment. *Scientific Reports* 2021; **11**, 11312.

[25] P Phatai and CM Futalan. Characteristics of cerium-aluminum-manganese mixed oxides and their performance in adsorbing methyl violet dye from an aqueous solution. *Desalination and Water Treatment* 2017; **62**, 257-266.

[26] S Kamonwannasit, CM Futalan, P Khemthong, T Butburee, A Karaphun and P Phatai. Synthesis of copper-silver doped hydroxyapatite via ultrasonic coupled sol-gel techniques: structural and antibacterial studies. *Journal of Sol-Gel Science and Technology* 2020; **96(2)**, 452-463.

[27] FA Akgul, G Akgul, N Yildirim, HE Unalan and R Turan. Influence of thermal annealing on microstructural, morphological, optical properties and surface electronic structure of copper oxide thin films. Materials Chemistry and Physics 2014; **147(3)**, 987-995

[28] F Arshad, A Munir, QQ Kashif, TU Haq, J Iqbal, F Sher and I Hussain. Controlled development of higher-dimensional nanostructured copper oxide thin films as binder free electrocatalysts for oxygen evolution reaction, *International Journal of Hydrogen Energy* 2020; **45(33)**, 16583-16590.

[29] VDCG Videira, BN Harada, VG Vital, RAGD Silva, SPD Vasconcellos and DS Pellosi. Structural and antibacterial evaluation of copper, silver, and bimetallic silver/copper nanoalloys synthesized in chitosan biopolymer. *Next Materials* 2024; **3**, 100071.

[30] V Sudha, G Murugadoss and R Thangamuthu. Structural and morphological tuning of Cu-based metal oxide nanoparticles by a facile chemical method and highly electrochemical sensing of sulphite. *Scientific Reports* 2021; **11**, 3413.

[31] TC Kaspar, T Droubay, SA Chambers and PS Bagus. Spectroscopic evidence for Ag(III) in highly oxidized silver films by x-ray photoelectron spectroscopy. *The Journal of Physical Chemistry C* 2010; **114(49)**, 21562-21571.

[32] P Prieto, V Nistor, K Nouneh, M Oyama, M Abd-Lefdil and R Diaz. XPS study of silver, nickel and bimetallic silver–nickel nanoparticles prepared by seed-mediated growth. *Applied Surface Science* 2012; **258(22)**, 8807-8813.

[33] K Bialik-Was, KN Raftopoulos and K Pielichowski. Alginate hydrogels with aloe vera: The effects of reaction temperature on morphology and thermal properties. *Materials* 2022; **15(3)**, 748.

[34] H Wang, J Liu, X Fan, J Ren, Q Liu and B Kong. Fabrication, characterisation, and application of green crosslinked sodium alginate hydrogel films by natural crab-shell powders to achieve drug sustained release. *LWT* 2022; **171**, 114147.

[35] Y Dong, D Sang, C He, X Sheng and L Lei. Mxene/alginate composites for lead and copper ion removal from aqueous solutions. *RSC Advances* 2019; **9(50)**, 29015-29022.

[36] W Lee and K Tsao. Effect of silver nanoparticles content on the various properties of nanocomposite hydrogels by in situ polymerization. *Journal of Materials Science* 2010; **45(1)**, 89-97.

[37] GR Deen and V Chua. Synthesis and properties of new "Stimuli" responsive nanocomposite hydrogels containing silver nanoparticles. *Gels* 2015; **1(1)**, 117-134.

[38] HA Ali and NJ Hameed. The study of the particle size effect on the physical properties of TiO_2/cellulose acetate composite films. *Journal of the Mechanical Behavior of Materials* 2022; **31(1)**, 150-159.

[39] SA Alobaid, S Shrestha, M Tasseff, B Wang, MLV Hoek and PK Dutta. Activity of silver-zinc nanozeolite-based antibiofilm wound dressings in an *in vitro* biofilm model and comparison with commercial dressings. *Discover Nano* 2025; **20(1)**, 26.